

Spin-orbital glass transition in a model of a frustrated pyrochlore magnet without quenched disorder

Kota Mitsumoto,¹ Chisa Hotta,² and Hajime Yoshino^{3,1}

¹*Graduate School of Science, Osaka University, Toyonaka, Osaka 560-0043, Japan*

²*Department of Basic Science, University of Tokyo, Tokyo 153-8902, Japan*

³*Cybermedia Center, Osaka University, Toyonaka, Osaka 560-0043, Japan*

We show theoretically that spin and orbital degrees of freedom in the pyrochlore oxide $Y_2Mo_2O_7$, which is free of quenched disorder, can exhibit a simultaneous glass transition, working as dynamical disorder for each other. The interplay of spins and orbitals is mediated by the Jahn-Teller lattice distortion that selects the choice of orbitals, which then generates variant spin exchange interactions ranging from ferromagnetic to antiferromagnetic ones. Our Monte Carlo simulations detect the power-law divergence of the relaxation times and the negative divergence of both the magnetic and dielectric nonlinear susceptibilities, resolving the long-standing puzzle on the origin of the disorder-free spin glass.

Glass formation is a generic phenomenon that emerges in strongly frustrated systems [1], ranging from super-cooled molecular liquids and densely packed soft-matters [2–5] to geometrically frustrated spin systems on kagome [6–10] and pyrochlore lattices [7, 11–20]. Frustration suppresses ordinary long-range orders and stabilizes liquid/paramagnetic states down to unusually low temperatures where the effect of many-body interactions become dominant. In sharp contrast to normal liquids at higher temperatures, molecules in super-cooled liquids can flow only through collective motions because of the strong inter-molecular interactions. In classical antiferromagnets on triangular, kagomé and pyrochlore lattices, the frustration among interactions caused by the lattice geometry precludes the possibility of all bonds to be simultaneously satisfied in energy [21]. An outstanding open question there is whether truly thermodynamic glass transitions, for example the putative Kauzmann transition of super-cooled liquids [22], are possible. At present such ideal glass transitions is attained only theoretically in unphysical limits of infinitely large dimensions for some super-cooled liquids [23–25] or spin systems with infinitely large number of spin components [26].

In realistic three-dimension, a true thermodynamic glass transition is established only in lattice systems with quenched disorder added on top of the frustration [27–29]. Theoretically, this spin glass(SG) is found in the Edwards-Anderson model [30, 31] based on both Ising [32–34] and Heisenberg spins [35–38].

The next fundamental question is whether the SG transition can be sustained even when such quenched disorder is switched off. It is known experimentally that some of the disorder-free pyrochlore magnets exhibit a sharp SG transition [7, 11–18], which is indistinguishable from the conventional one with quenched disorder [27–29]. The divergence of nonlinear susceptibility [14] establishes this phase as SG. In contrast, any of the theories available at present does not allow for the 3D SG without quenched disorder.

This Letter aims to clarify the origin of the SG transition in the disorder-free pyrochlore magnets by constructing a realistic model consisting of two key degrees of freedom of the system, i. e. spins and orbitals which are coupled through a Jahn-Teller (JT) lattice distortion which modifies the super-exchange interactions between the spins dynamically. The two degrees of freedom, if decoupled, live in highly degenerate energy landscapes of their own, due to the strong geometrical frustration, so that they remain in their liquid/paramagnetic states at all temperatures. Through the coupling they correlate producing dynamical disorder for each other and create an emergent rugged free-energy landscape. Our extensive MC simulation uncovers an unprecedented thermodynamic glass transition where the two degrees of freedom simultaneously freeze cooperatively.

The prototypical materials for our theory are the pyrochlore oxides, $A_2Mo_2O_7$ ($A = Ho, Y, Dy, Tb$), which are insulating and show a SG transition at around 20 K [15, 16, 39–42]. The magnetic ions Mo^{4+} ($4d^2, S = 1$) sit on the vertices of the corner shared tetrahedra (see Fig. 1(a)), and the interactions between them are antiferromagnetic, whose underlying microscopic mechanism is the superexchange mediated by the O^{2-} ions [43]. It has been established that the classical spin model with purely antiferromagnetic nearest neighbor interactions on the pyrochlore lattice remains nonmagnetic down to zero temperature because of the strong frustration effect [44, 45], not providing any hint of the SG transitions observed in experiments.

Very recently, some salient features of the local lattice distortions in $Y_2Mo_2O_7$ [19] were uncovered experimentally. The analysis based on the neutron pair-distribution function data suggests that the Mo^{4+} ions are locally displaced towards (*in*) or away from (*out*) the centers of Mo_4 tetrahedra (see Fig. 1(a)), explaining well a large variance of the Mo-Mo distances observed in the x-ray absorption study [20]. A natural mechanism of distortion is the JT effect that lowers the electrostatic energy

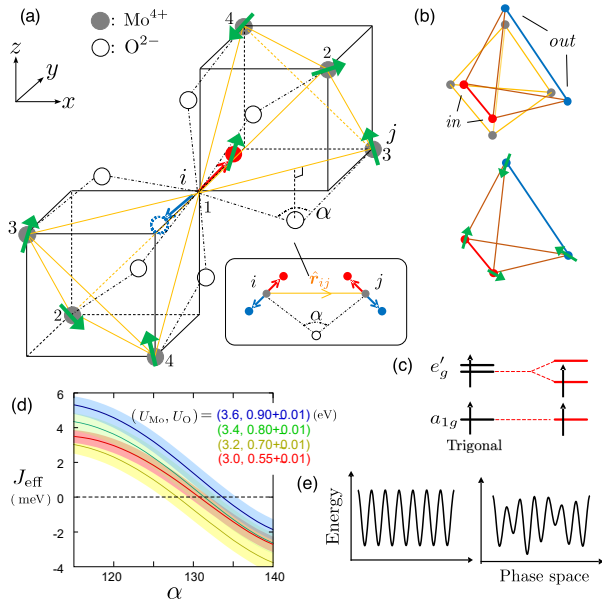


FIG. 1. (a): O^{2-} ions and magnetic Mo^{4+} ions around the i site, where the numbers 1-4 are the sublattice indices of Mo^{4+} ions. Red and blue dashed circles represent the positions of the Jahn-Teller distorted i ion. Spins on a pair of Mo^{4+} ions (i, j) interact through the O^{2-} ion as shown in the inset panel, where alpha is the Mo-O-Mo angle and \hat{r}_{ij} is the unit vector in the $i \rightarrow j$ direction. (b): Ice-type displacements of the Mo tetrahedron. The different color bonds represent different exchange interactions. (c): Lifting of the orbital degeneracy of e'_g by the JT effect. (d): α -dependence of the effective exchange interaction for typical on-site Coulomb interactions on Mo and O ions U_{Mo} and U_O (see SI). The shaded regions are the variance of J_{eff} when U_O is varied in the range of ± 0.01 . (e): Schematic pictures of the energy landscape of ice-type displacements (Top) and modified one by the coupling between the spin and lattice distortion.

of the Mo ion lifting its orbital degeneracy (Fig.1(c)) (See SI).

The displacements of the four Mo^{4+} ions on each tetrahedron possibly follow the 2-in-2-out rule, i. e. the ice-rule (see Fig. 1(a,b)), generating huge numbers of ionic configurations over the system equivalent in their JT energies. Such distortions thus do not lead to any long-range structural ordering.

It is empirically known [46] that the exchange interaction may vary significantly and even changes its sign, depending on the degree of the Mo-O-Mo angle α [43]. Indeed, the angle evaluated from the variance of the displacements of the Mo ions distributes in the range $\alpha = 116^\circ$ and 139° , which is large enough to change the sign of the interaction (Fig.1(d)) (See SI). Then, depending on the configurations of the local lattice distortion in space, the magnetic exchange interaction may acquire a random distribution with finite variances. This can be thought of as follows; If we consider the Jahn-Teller Hamiltonian including only the lattice degrees of free-

dom, the energy landscape should be such that all the ice-rules give the energy minima of the same height (see Fig.1(d)) [47, 48]. In putting spins on the ice-type displaced vertices, its energy landscape is modified to an irregular one with random valley structures, since the variance of the spin interactions from ferro to antiferromagnetic ones add different energies to each ice configuration. We verify the above picture showing numerically that the spin and lattice distortions simultaneously undergo a glass transition and freeze into the aperiodic, irregular types of configuration. Since the randomly frozen lattice distortions indicate the randomly selected orbital configurations, we call it a *spin-orbital glass*.

As a natural description of the material faithful to the experimental observations, we introduce a disorder-free spin model including not only the classical Heisenberg spins \mathbf{S}_i ($i = 1, 2, 3, \dots, N$) for the magnetic moments of the Mo^{4+} ($4d^2, S = 1$) ions but also the degree of lattice distortion of the Mo ions σ_i represented as vectors taking two discrete values, $\sigma_i = \sigma_i \hat{e}_\nu$. Here, $\sigma_i = \pm 1$ corresponds to either *in* or *out* depending on the direction of \hat{e}_ν which is the unit vector in the $[111]$, $[\bar{1}\bar{1}\bar{1}]$, $[\bar{1}\bar{1}1]$ and $[\bar{1}1\bar{1}]$ directions, respectively for the sub-lattices $\nu = 1, 2, 3, 4$ which the i -th spin belongs to (See Fig. 1.(a)). The Hamiltonian is given by

$$H = \sum_{\langle ij \rangle} J_{\sigma_i, \sigma_j} \mathbf{S}_i \cdot \mathbf{S}_j - \epsilon \sum_{\langle ij \rangle} \sigma_i \cdot \sigma_j \quad (\epsilon > 0) \quad (1)$$

with

$$J_{\sigma_i, \sigma_j} = J[1 + \delta(\hat{r}_{ij} \cdot \sigma_i + (-\hat{r}_{ij}) \cdot \sigma_j)] \quad (\delta > 0), \quad (2)$$

The first term in Eq. (1) represents the exchange interaction whose coupling constant J_{σ_i, σ_j} depends on the angle of Mo-O-Mo bond. This form is constructed in a way to reproduce the values of J_{eff} derived microscopically from the perturbation process on the Kanamori-type of Hamiltonian (see SI). As shown in Fig. 1 (d), for realistic values of the on-site Coulomb interactions on Mo^{4+} and O^{2-} ions [43, 49], J_{eff} changes its sign within the experimentally observed range of the Mo-O-Mo angle $\alpha = 116^\circ - 139^\circ$. This is modeled by Eq. (2) as such that $J_{\sigma_i, \sigma_j} = (1 + 2\tilde{\delta})J$ (*in, in*), J (*in, out*), $(1 - 2\tilde{\delta})J$ (*out, out*), where $\tilde{\delta} = \sqrt{6}\delta/3$ (See Fig. 1.(b)). The second term of Eq. (1) represents the elastic energy of the Mo^{4+} displacement. The elastic energy is minimized if a Mo^{4+} tetrahedron satisfies the ice-rule. More precisely, the elastic energy of each bond takes $\epsilon \sigma_i \cdot \sigma_j = -\epsilon/3$ if both displacements are *out* or *in*, otherwise $+\epsilon/3$. [50] There are three parameters in this system; $\tilde{T} = k_B T/J$ is the dimensionless temperature, $\tilde{\epsilon} = \epsilon/3J$ the ratio of the energy scales between the exchange interaction and the elastic energy of the displacement (hereafter we call them simply as T , ϵ , δ). At $\epsilon \rightarrow \infty$, the lattice distortion becomes static. In the following analysis, we mainly focus on a representative system at $\delta = 1.5, \epsilon = 0.6$.

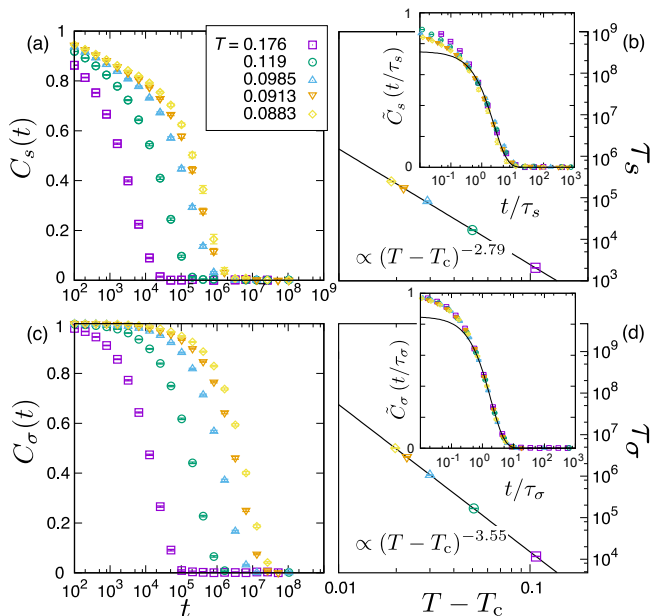


FIG. 2. Dynamical observables for $L = 6$. (a): Spin auto-correlation function. (b): Typical relaxation time of spin variables. (c): Orbital auto-correlation function. (d): Typical relaxation time of orbital variables. The black solid lines in the figure (b) and (d) denote the fits by $\tau = A(T - T_c)^{-z\nu}$ with $(A, T_c, z\nu)_s = (3.99(89), 0.0695(19), 2.79(12))$ and $(A, T_c, z\nu)_\sigma = (4.27(31), 0.0686(5), 3.55(4))$ by using the least squares method. Insets: Scaling plots of auto-correlation functions using their relaxation times. The solid lines represent the exponential fits.

We consider the periodic systems of cubic geometry consisting of L^3 unit cells with totally $N = 16L^3$ spins, and perform 120 statistically independent runs for the system size $L = 4, 5, 6, 8$, evaluating the averages and mean-squared errors of observable. To equilibrate the system we made a combined use of the exchange Monte Carlo method [51, 52], conventional and loop [53] update for lattice variables, Metropolis-Reflection [54] and over-relaxation [55] update for spin variables. However, to study the relaxational dynamics, we switched to single-spin-flip method after the equilibration. (see SI) We took 3×10^7 Monte Carlo steps for both equilibration and for taking thermal averages $\langle \dots \rangle_{\text{eq}}$.

To explore spin and orbital freezing we examined the auto-correlation functions (ACFs) for both degrees of freedom $C_s(t) = N^{-1} \sum_{i=1}^N \mathbf{S}_i(t) \cdot \mathbf{S}_i(0)$ and $C_\sigma(t) = N^{-1} \sum_{i=1}^N \boldsymbol{\sigma}_i(t) \cdot \boldsymbol{\sigma}_i(0)$ measured in equilibrium. The behavior of the spin and orbital ACFs are shown in Figs. 2(a) and 2(c). Both ACFs indicate the slowing down of the dynamics. As a quantitative measure of dynamics, we define the relaxation times $\tau_s(T)$ and $\tau_\sigma(T)$ for each degree of freedom as the time-scale such that the ACFs decrease down to 0.5, which are evaluated as shown in Figs. 2(b) and (d). Both relaxation times diverge at the same temperature $T_c \approx 0.07$ with power laws although

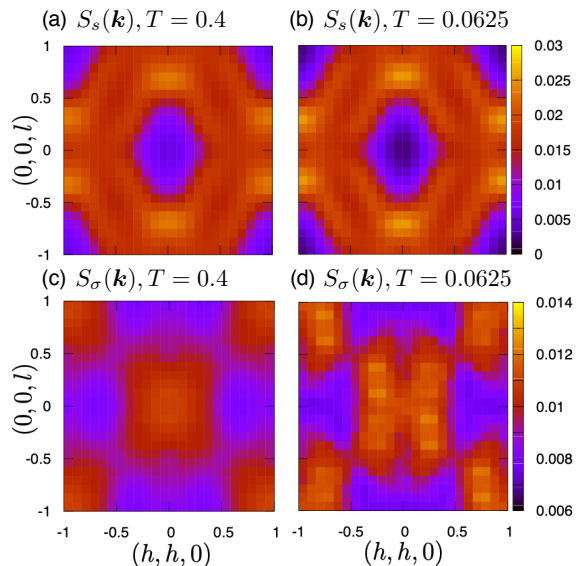


FIG. 3. Structure factors of the spins (a),(b) and orbitals (lattice distortions) (c),(d) on the $(h, h, l)/\pi$ plane for $L = 6$. Panels (a) and (c) are for $T = 0.4$ while (b) and (d) are for $T = 0.0625$. Pinch points can be seen, for example at $(1/2, 1/2, 1/2)$, at low temperatures.

their exponents differ. This suggests that the spin and orbital are frozen simultaneously. We checked that there is no finite size effect within the time scale which we analyzed. We also analyzed data at $\epsilon = 0.65$ and obtained consistent results. (See SI). In the insets of Figs. 2(b) and 2(d) we show the scaling plots of ACFs assuming a scaling form, $C(t, T) = \tilde{C}(t/\tau(T))$, which is clearly satisfied. The scaling functions turn out to be well fitted by simple exponentials. We note that the relaxation function in the Edwards-Anderson models in the paramagnetic phase is more complicated [32, 56] presumably due to Griffith singularity [57].

To get further insights we analyzed the static-structure factors of spins and lattice distortions defined respectively as $S_s(\mathbf{k}) = N^{-1} |\sum_{i=1}^N e^{-i\mathbf{k} \cdot \mathbf{r}_i} \mathbf{S}_i \cdot \mathbf{S}_i|$ and $S_\sigma(\mathbf{k}) = (4N)^{-1} |\sum_{i=1}^4 \sum_{j=1}^N e^{-i\mathbf{k} \cdot (\mathbf{r}_j - \mathbf{r}_i)} \boldsymbol{\sigma}_i \cdot \boldsymbol{\sigma}_j|$, where \mathbf{k} is a wave vector. In figures 3(a) and 3(b) we show $S_s(h, h, l)$ measured above and below T_c , which show no notable differences. No Bragg peaks are observed below T_c , indicating that there is no magnetic long range order. In Figs. 3(c) and 3(d), we also find no sign of long range order in the lattice distortions. The pinch-points similar to those observed in spin-ice systems [48][58] can be seen. The pinch-points reflect the fraction of tetrahedra that satisfy the ice-rule which increases smoothly with decreasing temperature without any anomaly at the transition temperature T_c . (see SI).

The present SG transition can be detected by the two thermodynamic quantities. One is the nonlinear mag-

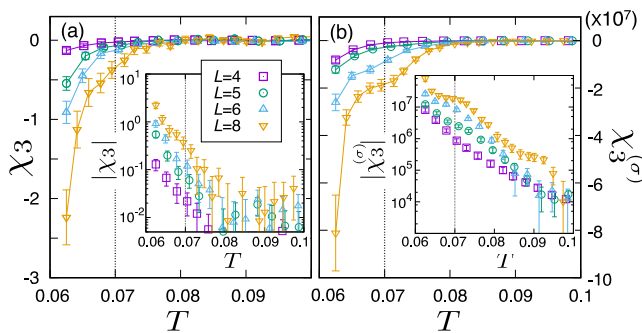


FIG. 4. (a), (b): Size dependence of nonlinear magnetic and dielectric susceptibilities (Insets: logarithmic scale of absolute values). The dashed line represents the freezing temperature $T_c \approx 0.07$ determined by the auto-correlation function.

netic susceptibility,

$$\chi_3 = \frac{1}{3} \sum_{\mu} \left. \frac{\partial^3 \langle m_{\mu} \rangle_{\text{eq}}}{\partial h_{\mu}^3} \right|_{h_{\mu} \rightarrow 0}, \quad (3)$$

where $m_{\mu} = N^{-1} \sum_{i=1}^N S_{i\mu}$ and h_{μ} are the magnetization and the magnetic field, respectively, in the μ -direction ($\mu = x, y, z$). The other is the nonlinear dielectric susceptibility,

$$\chi_3^{\sigma} = \frac{1}{4} \sum_{\nu} \left. \frac{\partial^3 \langle p_{\nu} \rangle_{\text{eq}}}{\partial E_{\nu}^3} \right|_{E_{\nu} \rightarrow 0}, \quad (4)$$

where $p_{\nu} = N^{-1} \sum_{i=1}^N \sigma_i \cdot \hat{e}_{\nu}$ is the dielectric polarization in the \hat{e}_{ν} -direction and E_{ν} is the electric field. Fortunately, the since Mo^{4+} ion has an electric charge, the fluctuation of the orbital glass ordering can be detected electrically. Thus, the two quantities are measurable in laboratories and allow a direct comparison between theories and experiments. In conventional theories [31, 59], one often analyzes the SG susceptibility, χ_{SG} , which is proportional to χ_3 . Although χ_{SG} is much easier to calculate with better accuracy in the presence of quenched disorder by using the overlap between two independent replicas, it is not convenient for our model, since the Hamiltonian is translationally invariant so that the replicas usually do not overlap.

Figure 4(a) shows χ_3 as a function of temperature for several system size L . In overall, it takes the negative value, and from slightly above T_c , its amplitude starts to grow rapidly in lowering the temperature. This growth is enhanced for larger L , strongly suggesting that the divergence of χ_3 remains in the thermodynamic limit, which is consistent with the experimental observation in $\text{Y}_2\text{Mo}_2\text{O}_7$. Similar behavior is observed for $\chi_3^{(\sigma)}$, indicating the freezing of the orbital degrees of freedom into a disordered state.

Let us discuss the relevance of our results with experiments. The existence of the SG transition itself is already

established in $\text{Y}_2\text{Mo}_2\text{O}_7$ and its families, and although its origin has not been understood, a recent analysis showed that the lattice distortions possibly plays a certain role in the glass transition. Our model is constructed based on this finding by including the direct coupling between the lattice distortion and the spin. The two degrees of freedom simultaneously undergo a glass transition, indicating that they generate an effect of dynamical randomness to each other. Experiments can test our scenario by examining whether the nonlinear dielectric susceptibility diverges in the vicinity of T_c , where already the nonlinear magnetic susceptibility shows the divergence. Previously, the orbital-glass transition was observed in the FeCr_2S_4 , where the dielectric spectroscopy measurement played a major role, detecting the slowing down of orbital dynamics [60]. Similar techniques shall be applied to the pyrochlore materials and in addition to that the ZFC/FC anomaly [15] shall be tested in linear dielectric response of the pyrochlore materials.

Let us finally comment on the scenario often posed experimentally, which expects the freezing of the orbital degrees of freedom at a higher temperature than the SG transition [19, 20]. Once the orbital configuration is frozen, our model is reduced to the standard EA model of Heisenberg spins with quenched randomness on a pyrochlore lattice, which is known to exhibit a SG transition [61, 62]. Actually, if we increase ϵ in Eq.(1), the ice-rule configuration of orbitals is selected at the higher temperature, which is detected by the broad peak in the heat capacity (see SI). However, this peak does not mean the transition but a crossover; Below that temperature, the orbitals are still dynamically fluctuating among huge numbers of quasi-degenerate ice-rule configurations. In lowering the temperature, the orbital dynamics naturally slows down but without any thermodynamic anomaly such as usual spin ices [63]. Interestingly, at a lower temperature the heat capacity shows a second peak (see SI) which should be attributed to coupling between the spin and lattice distortions. In our scenario, we anticipate the thermodynamic spin-orbital glass transition at around that temperature.

Some other effect such as the spin-orbit interaction [49], the spin-phonon coupling and longer range interactions, which are not included in our model, may be needed to reproduce more precisely the experimental measurements, whereas our findings proved that the interplay of nearest-neighbor interactions and the dynamical JT distortions can solely drive the system to the glass transition. The present model can be further applied to other SG frustrated magnets such as $\text{Tb}_2\text{Mo}_2\text{O}_7$ whose magnetic ion is JT active.

To summarize, we introduced the realistic model without quenched randomness consisting of spin and orbital degrees of freedom, that shows the thermodynamic glass transition for the first time in the finite dimensional periodic lattice. We performed the dynamical simulations

in the equilibrium and found that the relaxation times of both spins and orbitals show a power-law divergence at the same temperature, T_c . The nonlinear magnetic susceptibility and the nonlinear dielectric susceptibility together show negative divergence at around T_c , signaling the simultaneous glass transition of these two degrees of freedom. The former is consistent with the experiments already performed in the pyrochlore oxide, $Y_2Mo_2O_7$, whereas the latter can be tested in the near future to fix the long standing problem on the origin of the SG transition in this disorder free crystalline solid.

This work was supported by KAKENHI (No. 19H01812, 17K05533, 17K05497, 18H01173, 17H02916) from MEXT, Japan. The computation in this work has been done using the facilities of the Supercomputer Center, the Institute for Solid State Physics, the University of Tokyo, OCTOPUS and supercomputer system SX-ACE at the Cybermedia Center, Osaka University.

Microscopic justification of the effective model

In a pyrochlore oxide $\text{Y}_2\text{Mo}_2\text{O}_7$, magnetic ion $\text{Mo}^{4+}(4d^2)$ is affected by trigonal crystal field, and its triply t_{2g} orbitals split into a single a_{1g} orbital and doubly e'_g orbitals, where a_{1g} has the lower energy than e'_g . The spins of two electrons on Mo^{4+} form an effective $S = 1$ following Hund's rule. This is because the magnitude of energy splitting between a_{1g} and e'_g is smaller than the strength of Hund's coupling. [43] We further take account of the Jahn-Teller lattice distortion, which is observed experimentally [19, 20]. Ref.[19] shows that each Mo^{4+} moves away from the center of the tetrahedron, and accordingly, the Mo-O-Mo angle varies from its equilibrium position $\alpha = 127^\circ$ to 116° for the in-in bond and 139° for the out-out bond. We checked that the change of the angle is large enough to give the different sign of the exchange interaction as in the following.

We consider an extended Kanamori Hamiltonian consisting of d -orbitals $a = |a_{1g}\rangle, |e'_{g+}\rangle, |e'_{g-}\rangle$ of Mo^{4+} ions and p -orbitals $b = |p(X)\rangle, |p(Y)\rangle, |p(Z)\rangle$ on the O^{2-} ion. As shown in Fig. S6, we consider two adjacent Mo^{4+} ions, A and B, and the relative position of the degenerate three p -orbitals whose quantization axis is defined as such that it is line symmetric with respect to A and B. The Hamiltonian is given as

$$\begin{aligned} \mathcal{H} = & - \sum_{i=A,B} \sum_{a,b} \sum_{\sigma} t_{a,b} \left(c_{ia\sigma}^\dagger c_{ob\sigma} + c_{ob\sigma}^\dagger c_{ia\sigma} \right) + \sum_{i=A,B} \sum_a \Delta e_a \sum_{\sigma} c_{ia\sigma}^\dagger c_{ia\sigma} \\ & + \sum_{i=A,B} \sum_{a,a'} \sum_{\sigma,\sigma'} \frac{K(a,a') - \delta_{\sigma,\sigma'} J(a,a')}{2} c_{ia\sigma}^\dagger c_{ia\sigma} c_{ia'\sigma'}^\dagger c_{ia'\sigma'} + \frac{U_o}{2} \sum_b c_{ob\sigma}^\dagger c_{ob\sigma} c_{ob'\sigma'}^\dagger c_{ob'\sigma'}, \end{aligned} \quad (5)$$

where $c_{la\sigma}/c_{la\sigma}^\dagger$ are the annihilation/creation operators of the a -orbital of either the Mo-site ($l = A, B$) or O-site ($l = o$) with spin σ . The transfer integral $t_{a,b}$ in the first term are those between a -orbital of Mo($4d$) and b -orbital of O($2p$), which depends on both the distances between ions and the Mo-O-Mo angle α [64]. We calculated $t_{a,b}$ based on the Slater-Koster parameter, as presented in Table. 5. The hopping between $p(Y)$ and any Mo($4d$) orbitals are relatively small and does not depend much on α , thus are neglected.

The second term represents the excitation energy from O($2p$) to Mo($4d$) and we adopt $\Delta e_{a_{1g}} = 2.0$ and $\Delta e_{e'_{g\pm}} = 2.5$ taken from the first principles band calculation in Ref.[43]. The third and fourth terms are the on-site Coulomb interactions on Mo^{4+} and O^{2-} , respectively. $K(\alpha, \alpha')$ and $J(\alpha, \alpha')$ are the Coulomb and exchange integrations which are described by the Slater-Condon parameters F^0, F^2 and F^4 . We adopt $F^2 = 4.52$ and $F^4/F^2 = 0.63$ [43]. We leave $F^0 = U_{\text{Mo}}$ and U_o , which represent the strength of the on-site Coulomb interactions on the Mo and O ions respectively, as parameters.

We start from the strong coupling limit, $t_{a,b} \ll U_{\text{Mo}}, U_o, \Delta e_a$, where the Mott insulating ground state consists of fully occupied O($2p$) orbitals and the A/B ions each having two electrons that occupy a_{1g} and either of e'_{g+}/e'_{g-} (See

	$\alpha = 116^\circ$	$\alpha = 127^\circ$	$\alpha = 139^\circ$
$ t_{p(X),a_{1g}} ^2$	0.951913	0.561214	0.151767
$ t_{p(X),e'_{g\pm}} ^2$	1.97879	2.42526	2.69398
$ t_{p(Z),a_{1g}} ^2$	0.0580811	0.323847	0.738423
$ t_{p(Z),e'_{g\pm}} ^2$	0.97992	0.572566	0.216754

FIG. 5. The square of the transfer integral $|t|^2$ (eV^2) for three angles $\alpha = 116^\circ, 127^\circ, 139^\circ$ evaluated by the Slater-Koster parameter.

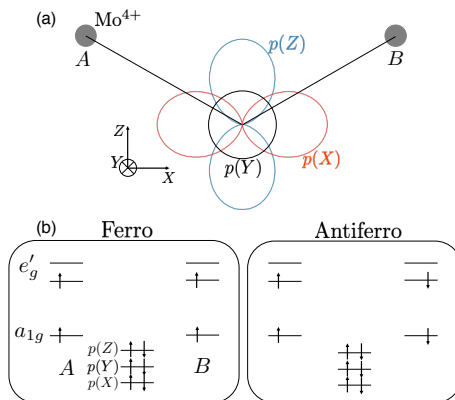


FIG. 6. (a) Relative positions between two Mo^{4+} ions (A,B) and O($2p$) orbitals. Since one can construct three degenerate p -orbitals in an arbitrary combination, we define the new orbitals $|p(X)\rangle, |p(Y)\rangle, |p(Z)\rangle$ in a symmetric manner in terms of A and B. (b): Electronic configurations of ferromagnetic and antiferromagnetic low energy Mott insulating states in the strong coupling limit of Eq.(S1).

Fig. S1 (a)). Since these two electrons on the same Mo($4d$) ions form the $S = 1$ triplet due to Hund's coupling, there are four different spin configurations $(S_A^z, S_B^z) = (\uparrow, \uparrow), (\uparrow, \downarrow), (\downarrow, \uparrow), (\downarrow, \downarrow)$ which we take as a low energy basis. The leading term which gives the effective exchange interaction $J_{\text{eff}} \mathbf{S}_A \cdot \mathbf{S}_B$ is obtained at the fourth of perturbation in terms of $t_{a,b}$. By considering all the perturbation processes of either of the two electrons on the p -orbitals each to hop to the empty orbitals on A and B ions and coming back, one can evaluate the energy gain $E_{\text{F/AF}}^{(4)}$ for the parallel and anti-parallel spin orientations of A and B ions. The effective exchange interaction is given by $J_{\text{eff}} = (E_{\text{F}}^{(4)} - E_{\text{AF}}^{(4)})/3$, where denominator 3 is from the effective spin $S = 1$. The fact that both $|t_{p(X),a_{1g}}|^2$ and $|t_{p(Z),e'_{g\pm}}|^2$ vary significantly with α affects the relative energy gain of $E_{\text{F}}^{(4)}$ and $E_{\text{AF}}^{(4)}$, the sign of J_{eff} also changes its sign at $\alpha \sim 127^\circ$, as we present in Fig. 1(d) in the main text.

Details of the Monte Carlo simulation

Here we explain the details of our Monte Carlo simulation. For updating lattice displacements σ_i ($i = 1, 2, 3, \dots, N$) we used the conventional single-spin-flip Metropolis method. However, it is hard to investigate the thermodynamic properties of the ice-type system at low temperature due to multiple energy minima with high energy barrier. Therefore, we also adopted a nonlocal update method called the loop algorithm. [53] The nonlocal update consists of two steps: (1) We look for the loop consisting of only *in-out* bonds. (2) We flip all the lattice displacements on the loop simultaneously with the acceptance rate determined by the Metropolis rule. Note that the energy contribution from the second term of the Hamiltonian remains unchanged in this update. For updating Heisenberg spins we used the Metropolis Reflection method [54] and the over-relaxation method. [55] In the Metropolis Reflection method, we prepare a plane dividing spin space into two equal parts randomly. To update a spin \mathbf{S}_i , a new candidate spin configuration \mathbf{S}'_i is created by reflecting \mathbf{S}_i by the plane. More precisely the sign of the perpendicular component to plane is changed. The reflection is performed with probability determined by Metropolis rule. In a unit Monte Carlo step (MCS), we try the update for all spins \mathbf{S}_i ($i = 1, 2, 3, \dots, N$) and apply the same plane to reflect all spins. In the over-relaxation method, we first calculate the effective magnetic field \mathbf{h}_{eff} around a spin \mathbf{S}_i , and then rotate the spin around \mathbf{h}_{eff} by an angle of π . A unit Monte Carlo step is consisted of the following steps.

1. Sequential single-spin flip for all lattice displacements with the conventional Metropolis method
2. L times loop update for lattice displacements
3. Calculating all the coupling constants J_{σ_i, σ_j}
4. Sequential single-spin flip for all Heisenberg spins with the Metropolis Reflection method
5. L times sequential single-spin flip for all Heisenberg spins with the over-relaxation method

Here L is the system size defined in the main text.

The equilibrium states were realized by the replica exchange method. [51, 52] We prepared 48 replicas for $L = 4, 5, 6$ and 72 replicas for $L = 8$. We determined the maximum temperature and the minimum temperature as $T_{\text{max}} = 0.400$ and $T_{\text{min}} = 0.0625$ respectively. We optimized the temperature set so that the exchange rate is independent of T . [52] We performed the trial to exchange the replicas with the interval 15 (MCS). Initial spin and lattice configuration for each replica were prepared a fully random configuration. MCSs for thermalization was determined as 3.0×10^7 (MCS) for all system sizes. Observations of physical quantities are made during additional 3.0×10^7 (MCS) to evaluate their thermal averages $\langle \dots \rangle_{\text{eq}}$ by their MCS averages.

In dynamical simulations in equilibrium, the initial configurations ($t = 0$ (MCS)) are created by above equilibration. In order to observe the natural time evolution we apply only the sequential single-spin flip for both degrees of freedom. A unit Monte Carlo step is consisted of the following steps.

1. Sequential single-spin flip for all lattice displacements with the conventional Metropolis method
2. Calculating all the coupling constants J_{σ_i, σ_j}
3. Sequential single-spin flip for all Heisenberg spins with the Metropolis Reflection method

Definitions of the non-linear magnetic and dielectric susceptibilities

Here we present the detailed definition of the non-linear susceptibilities we measured in our simulations. From fluctuation formulae we obtain the non-linear magnetic susceptibility as

$$\begin{aligned}\chi_3 &= \frac{1}{3} \sum_{\mu} \frac{\partial^3 \langle m_{\mu} \rangle_{\text{eq}}}{\partial h_{\mu}^3} \\ &= \frac{\beta^3 N^3}{3} \sum_{\mu} \left(\langle m_{\mu}^4 \rangle_{\text{eq}} - 4 \langle m_{\mu} \rangle_{\text{eq}} \langle m_{\mu}^3 \rangle_{\text{eq}} - 3 \langle m_{\mu}^2 \rangle_{\text{eq}}^2 + 12 \langle m_{\mu}^2 \rangle_{\text{eq}} \langle m_{\mu} \rangle_{\text{eq}}^2 - 6 \langle m_{\mu} \rangle_{\text{eq}}^4 \right).\end{aligned}\quad (6)$$

Within our Monte Carlo simulations of finite sized systems, odd order moments of the magnetization vanish due to the rotational symmetry, e.g. $\langle m_{\mu} \rangle_{\text{eq}} = \langle m_{\mu}^3 \rangle_{\text{eq}} = 0$. Hence we can evaluate it simply as,

$$\chi_3 = \frac{\beta^3 N^3}{3} \sum_{\mu} \left(\langle m_{\mu}^4 \rangle_{\text{eq}} - 3 \langle m_{\mu}^2 \rangle_{\text{eq}}^2 \right).\quad (7)$$

Similarly we evaluate the the non-linear dielectric susceptibility in the same manner as,

$$\chi_3^{(\sigma)} = \frac{\beta^3 N^3}{4} \sum_{\nu} \left(\langle p_{\nu}^4 \rangle_{\text{eq}} - 3 \langle p_{\nu}^2 \rangle_{\text{eq}}^2 \right).\quad (8)$$

Spin and orbital time auto-correlation functions

In main text, we present the results of the time auto-correlation functions of the spin and orbital at $\epsilon = 0.60$. The data suggest that spin and orbital degrees of freedom simultaneously freeze at $T_c \approx 0.07$. Here we show an additional data set obtained at $\epsilon = 0.65$. The scaling analysis of the data suggests a simultaneous glass transitions at $T_c \approx 0.086$. Notably, the exponents $z\nu$ agree with those obtained at $\epsilon = 0.6$ within the numerical accuracy, suggesting a universality.

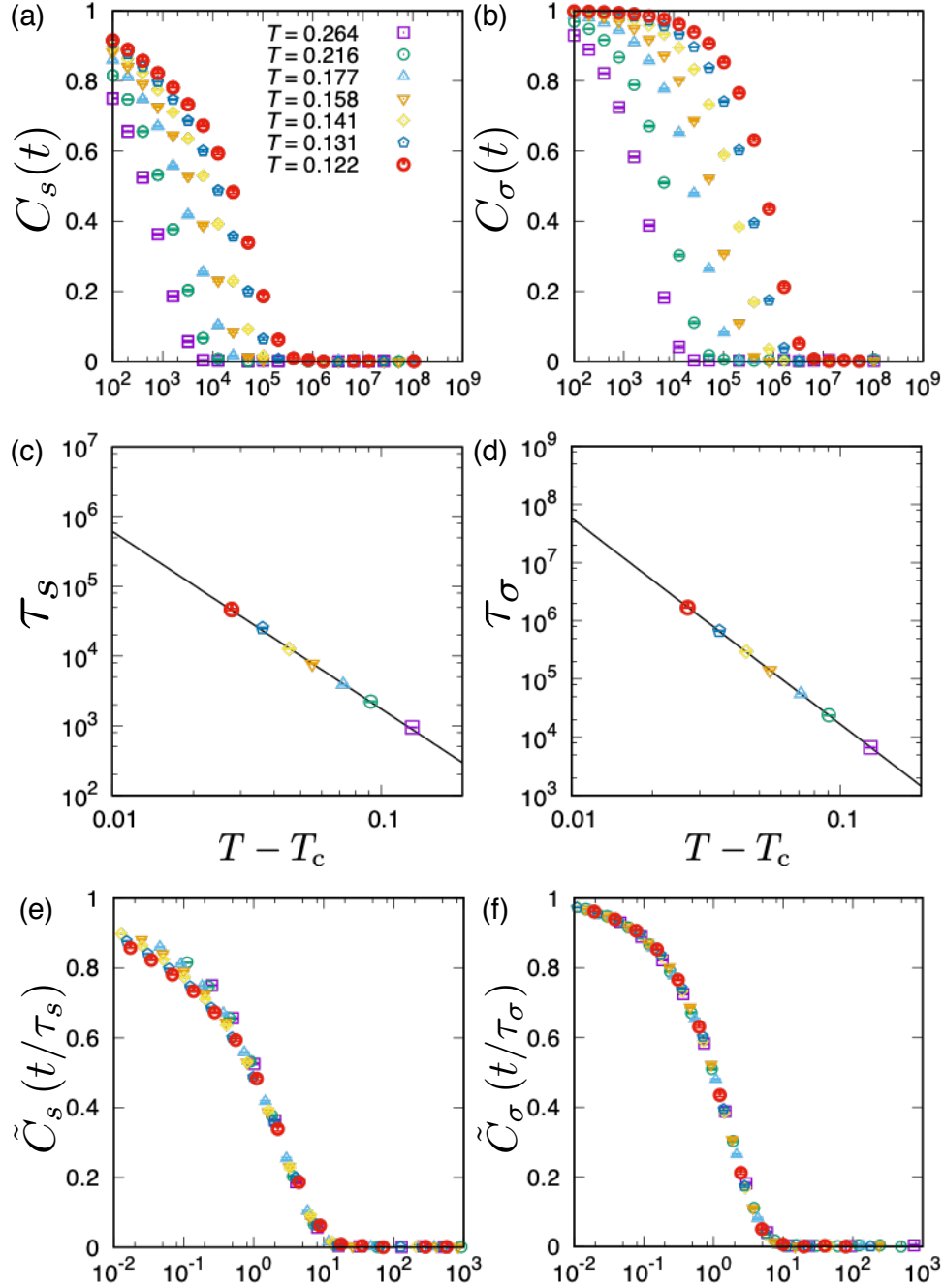


FIG. 7. Dynamical observables for $L = 5$, $\epsilon = 0.65$. (a): Spin auto-correlation function. (b): Orbital auto-correlation function. (c): Typical relaxation time of spin variables. (d): Typical relaxation time of orbital variables. The black lines in the figure (a) and (b) denote the fits by $\tau = A(T - T_c)^{-z\nu}$ with $(A, T_c, z\nu)_s = (4.91(154), 0.0855(26), 2.55(15))$ and $(A, T_c, z\nu)_\sigma = (4.78(21), 0.0862(5), 3.54(3))$ by using the least squares method. (e), (f): Scaling plots of spin and orbital auto-correlation function, respectively.

Heat capacity

We show below the temperature dependence of heat capacity for various ϵ . We can see a broad peak in the vicinity of spin glass transition temperature T_c , similarly to the observations in usual spinglass systems (for example see Chap 3.1.2 of [27]) and the pyrochlore SG [65]. One see that the dependence on the system size is very weak (see Fig. S3 (a)).

For larger ϵ , another broad peak emerges at higher temperatures (see Fig. S3 (c)), which can be interpreted as a reflection of the crossover from purely random phase to ice like phase. (see Fig. S4.)

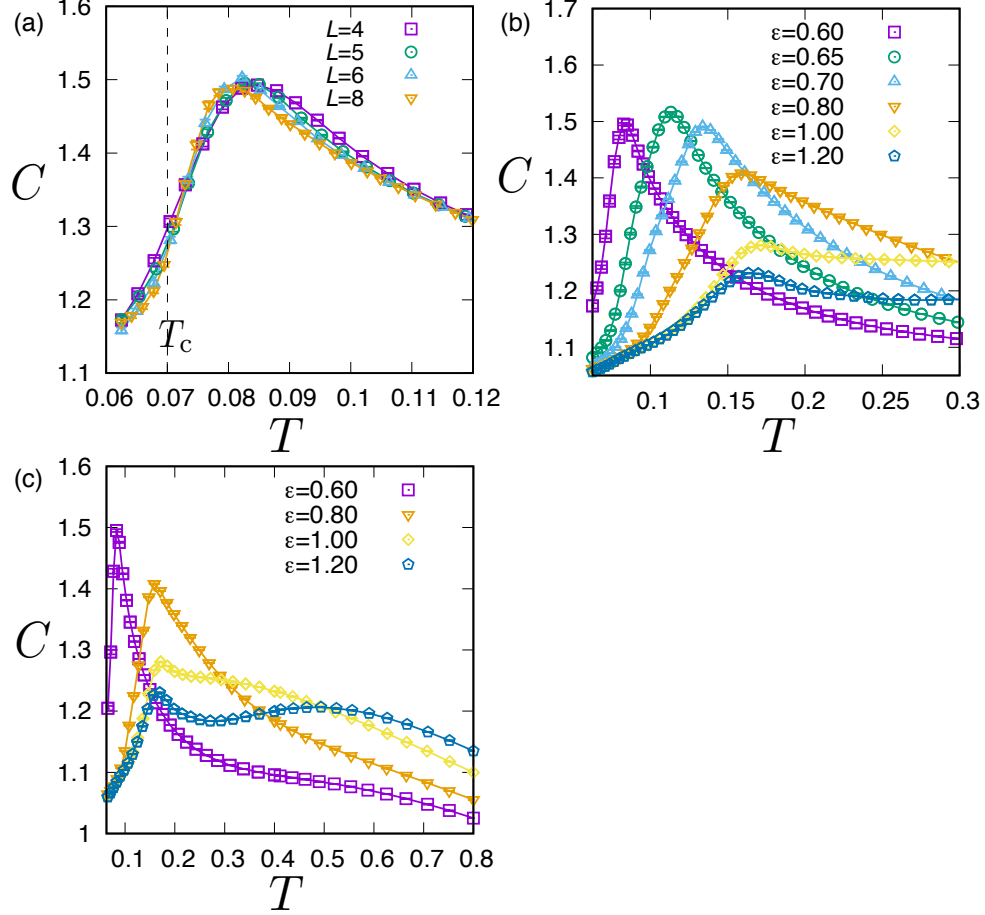


FIG. 8. Heat capacity calculated as $C = N^{-1}\beta^2(\langle E^2 \rangle_{\text{eq}} - \langle E \rangle_{\text{eq}}^2)$. (a): Size dependence at $\epsilon = 0.6$. (b): ϵ dependence for $L = 5$ in the narrow range of $T = 0.0625$ to $T = 0.3$. (c): ϵ dependence for $L = 5$ in the wide range of $T = 0.0625$ to $T = 0.8$.

Fraction of ice like lattice distortions

Fig. S4 shows the temperature-dependence of the fraction of ice like 2-in 2-out structure of the lattice distortions for various ϵ . It can be seen that the onset of ice like structure is gradual. The 2ndary peak of the heat-capacity observed at large ϵ (See Fig. S3(c)) can be interpreted as due to the onset of the ice like structures.

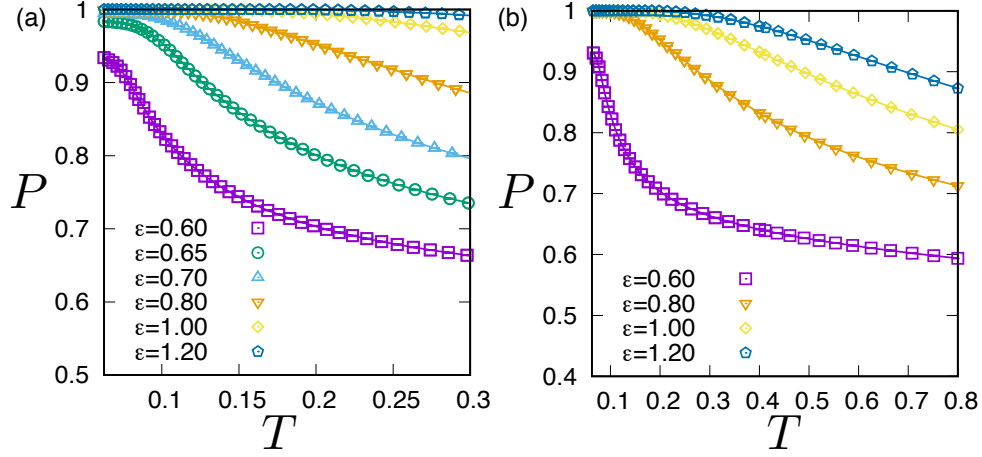


FIG. 9. Fraction of the ice structures given by $N_{2-in-2-out}/N_{\Delta}$. Here $N_{\Delta} = N_{\text{spin}}/2$ represents the number of all tetrahedra and $N_{2-in-2-out}$ represent the number of tetrahedra which are distorted into 2-in-2-out structures. (a): ϵ dependence for $L = 5$ in the narrow range of $T = 0.0625$ to $T = 0.3$. (b): ϵ dependence for $L = 5$ in the wide range of $T = 0.0625$ to $T = 0.8$.

Non-linear magnetic and dielectric susceptibilities

In the main text, we present the temperature dependence of magnetic and dielectric non-linear susceptibilities for $\epsilon = 0.60$. Here, we show them for various ϵ .

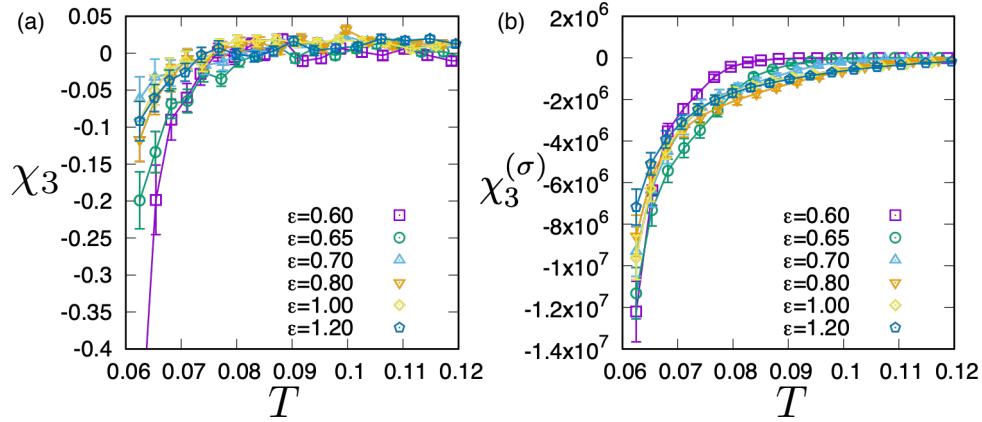


FIG. 10. (a): ϵ dependence of the non-linear magnetic susceptibility for $L = 5$. (b): ϵ dependence of the non-linear dielectric susceptibility for $L = 5$.

-
- [1] G. Tarjus, S. A. Kivelson, Z. Nussinov, and P. Viot, *Journal of Physics: Condensed Matter* **17**, R1143 (2005).
 [2] C. A. Angell, K. L. Ngai, G. B. McKenna, P. F. McMillan, and S. W. Martin, *Journal of Applied Physics* **88**, 3113 (2000).
 [3] F. Sciortino and P. Tartaglia, *Advances in Physics* **54**, 471 (2005).

- [4] A. Cavagna, *Physics Reports* **476**, 51 (2009).
- [5] L. Berthier and G. Biroli, *Reviews of Modern Physics* **83**, 587 (2011).
- [6] B. Martinez, F. Sandiumenge, A. Rouco, A. Labarta, J. Rodríguez-Carvajal, M. Tovar, M. Causa, S. Gali, and X. Obradors, *Physical Review B* **46**, 10786 (1992).
- [7] F. Ladieu, F. Bert, V. Dupuis, E. Vincent, and J. Hammann, *Journal of Physics: Condensed Matter* **16**, S735 (2004).
- [8] J. Hamp, R. Moessner, and C. Castelnovo, *Physical Review B* **98**, 144439 (2018).
- [9] L. F. Cugliandolo, L. Foini, and M. Tarzia, arXiv preprint arXiv:1909.12944 (2019).
- [10] S. K. Upadhyay, K. K. Iyer, and E. Sampathkumaran, *Journal of Physics: Condensed Matter* **29**, 325601 (2017).
- [11] M. Alba, J. Hammann, C. Jacoboni, and C. Pappa, *Physics Letters A* **89**, 423 (1982).
- [12] J. Greedan, M. Sato, X. Yan, and F. Razavi, *Solid state communications* **59**, 895 (1986).
- [13] J. Reimers, J. Greedan, R. Kremer, E. Gmelin, and M. Subramanian, *Physical Review B* **43**, 3387 (1991).
- [14] M. Gingras, C. Stager, B. Gaulin, N. Raju, and J. Greedan, *Journal of applied physics* **79**, 6170 (1996).
- [15] M. Gingras, C. Stager, N. Raju, B. Gaulin, and J. Greedan, *Physical review letters* **78**, 947 (1997).
- [16] J. Gardner and et al., *Physical review letters* **83**, 211 (1999).
- [17] H. Zhou, C. Wiebe, A. Harter, N. Dalal, and J. Gardner, *Journal of Physics: Condensed Matter* **20**, 325201 (2008).
- [18] T. Taniguchi, T. Munenaka, and H. Sato, in *Journal of Physics: Conference Series*, Vol. 145 (IOP Publishing, 2009) p. 012017.
- [19] P. Thygesen and et al., *Physical review letters* **118**, 067201 (2017).
- [20] C. Booth and et al., *Physical Review B* **62**, R755 (2000).
- [21] H. Diep *et al.*, (World Scientific, 2013).
- [22] W. Kauzmann, *Chem Rev* **43**, 219 (1948).
- [23] G. Parisi and F. Zamponi, *Reviews of Modern Physics* **82**, 789 (2010).
- [24] J. Kurchan, G. Parisi, and F. Zamponi, *Journal of Statistical Mechanics: Theory and Experiment* **2012**, P10012 (2012).
- [25] P. Charbonneau, J. Kurchan, G. Parisi, P. Urbani, and F. Zamponi, *Nature communications* **5** (2014).
- [26] H. Yoshino, *SciPost Physics* **4**, 040 (2018).
- [27] J. A. Mydosh, *Spin glasses: an experimental introduction* (CRC Press, 2014).
- [28] K. Binder and A. Young, *Reviews of Modern physics* **58**, 801 (1986).
- [29] H. Kawamura and T. Taniguchi, *Handbook of Magnetic Materials*, Vol. 24 (Elsevier, 2015) pp. 1–137.
- [30] S. Edwards and P. Anderson, *Journal of Physics F: Metal Physics* **5**, 965 (1975).
- [31] M. Mézard, G. Parisi, and M. Virasoro, Vol. 9 (World Scientific Publishing Company, 1987).
- [32] A. Ogielski, *Physical Review B* **32**, 7384 (1985).
- [33] R. N. Bhatt and A. Young, *Physical Review B* **37**, 5606 (1988).
- [34] N. Kawashima and A. Young, *Physical Review B* **53**, R484 (1996).
- [35] K. Hukushima and H. Kawamura, *Physical Review E* **61**, R1008 (2000).
- [36] L. Lee and A. Young, *Physical Review B* **76**, 024405 (2007).
- [37] D. X. Viet and H. Kawamura, *Physical review letters* **102**, 027202 (2009).
- [38] T. Ogawa, K. Uematsu, and H. Kawamura, (2019), arXiv:1912.02502 [cond-mat.dis-nn].
- [39] B. Gaulin, J. Reimers, T. Mason, J. Greedan, and Z. Tun, *Physical review letters* **69**, 3244 (1992).
- [40] S. Dunsiger and et al., *Physical Review B* **54**, 9019 (1996).
- [41] I. Kézsmárki and et al., *Physical review letters* **93**, 266401 (2004).
- [42] N. Hanasaki and et al., *Physical review letters* **99**, 086401 (2007).
- [43] I. Solov'yev, *Physical Review B* **67**, 174406 (2003).
- [44] J. Reimers, A. Berlinsky, and A. Shi, *Physical Review B* **43**, 865 (1991).
- [45] R. Moessner and J. Chalker, *Physical review letters* **80**, 2929 (1998).
- [46] The evaluation of the direct exchange interactions between Mo spins can be done based on the Hartree-Fock approach by assuming the orbital ordering, which gives a rough estimate of the sign of the interactions. We give a more detailed analysis by considering the dominant superexchange interactions for the insulating $\text{Y}_2\text{Mo}_2\text{O}_7$.
- [47] L. Pauling, Vol. 260 (Cornell university press Ithaca, NY, 1960).
- [48] S. Bramwell and M. Gingras, *Science* **294**, 1495 (2001).
- [49] H. Shinaoka, Y. Motome, T. Miyake, and S. Ishibashi, *Physical Review B* **88**, 174422 (2013).
- [50] This term is the simplified description of the energies of the classical elastic model whose lattice sites are connected by springs, for which one can easily find that the two-in two-out configurations give the lowest energy, consistent with the experimental findings.
- [51] K. Hukushima and K. Nemoto, *Journal of the Physical Society of Japan* **65**, 1604 (1996).
- [52] K. Hukushima, *Physical Review E* **60**, 3606 (1999).
- [53] R. Melko, B. den Hertog, and M. Gingras, *Physical review letters* **87**, 067203 (2001).
- [54] S. Pawig and K. Pinn, *International Journal of Modern Physics C* **9**, 727 (1998).
- [55] J. Alonso and et al., *Physical Review B* **53**, 2537 (1996).
- [56] H. Yoshino and H. Takayama, *EPL (Europhysics Letters)* **22**, 631 (1993).
- [57] A. Bray, *Physical review letters* **60**, 720 (1988).
- [58] Note however that here we don't multiply any scattering factor $|f(\mathbf{k})|$ to the structure factor.
- [59] D. Fisher and D. Huse, *Physical Review B* **38**, 386 (1988).
- [60] R. Fichtl and et al., *Physical review letters* **94**, 027601 (2005).
- [61] T. Saunders and J. Chalker, *Physical review letters* **98**, 157201 (2007).

- [62] H. Shinaoka, Y. Tomita, and Y. Motome, Physical review letters **107**, 047204 (2011).
- [63] L. Jaubert and P. Holdsworth, Nature Physics **5**, 258 (2009).
- [64] W. Harrison, (Courier Corporation, 2012).
- [65] N. Raju, E. Gmelin, and R. Kremer, Physical Review B **46**, 5405 (1992).